Chapter-6

Electrocatalytic activity of nickel oxide thin film

Publication: ***Manisha Chauhan, Ajay S. Bangwal, and Prabhakar singh, "Electrocatalytic activity of nickel oxide thin film: optimization of pH towards oxygen evolution reaction and oxygen reduction reaction". (communicated)***

CHAPTER 6: Electrocatalytic activity of nickel oxide thin film

6.1 Introduction

The use of hydrogen (H_2) gas as a clean, effective, and portable fuel has emerged as one of the alluring alternatives to traditional forms of energy consumption as the need of clean fuel increases and environmental concerns are becoming more widely recognised[259]. Therefore, there is a critical need to produce water splitting electrocatalysts that are more active, effective, stable, and affordable while also providing low overpotentials for the hydrogen and oxygen evolution reactions. In the previous chapter, the effects of oxygen reduction (ORR) and oxygen evolution reaction (OER) on the functionality of numerous electrochemical devices and storage systems has been already discussed.

Numerous important technological processes use metal oxides and their composites as electrocatalysts and catalysts due to their outstanding stability and high activity, in particular Ni and Co oxides for the OER in alkaline electrolyzers for a long time. The OER, which converts water molecules into molecular oxygen, is a key component of these activities. Traditionally, nickel electrodes are used in an alkaline medium, while platinum is typically used for oxygen evolution in an acidic medium. The scarcity and cost of Pt, hamper its commercialization for electrolysis. So for the solution, Ni and Ni based alloys have been studied as HER catalyst for their activity and stablity in alkaline solutions. However, it is still challenging to attain both high activity and stability matching those of Pt. Stoichiometric NiO has an octahedral Ni^{2+} and O^{2-} occupied cubic structure (Pm3m)[260]. Nickel, cobalt, and iron oxide electrodes [240], [261]–[263] are effective for OER in alkaline media. The best performance in acid and other solutions is shown by IrO_2 with or without RuO_2 [264]–[266].

Nickel oxide has been used in smart windows[267], [268], gas sensors [269] supercapacitors for energy storage[270] and electrochromic devices for application purpose.

Nanostructured oxides have special features that oxide semiconductor make them ideal for a variety of Novel applications, including lasers, smart windows, transparent conductors, and solid electrolytes. The characteristics of oxide materials at the nanoscale are different from those of bulk materials due to quantum and other size effects. The most of experimental research at this time are based on thin-film oxide materials, which are characterised by the presence of numerous grain boundaries between regions with different crystallographic orientations. Materials' properties are influenced by their grain size. The huge area of the grain boundary per unit weight of the material is related to this. NiO is a transition metal have wide range of application at nanoscale. Thin film of p-type semiconductor has application in opto-electronic devices.

The catalytic characteristics of nickelate-based systems were fully investigated in the previous chapters using the materials RP layered type materials i.e., $SmSrNiO_{4-\delta}$, $Sm_{2-x}Sr_xNiO_{4-\delta}$, and $Sm_{1-x}La_xSr_{1-x}Ca_xNiO_{4-\delta}$ in bulk and thin form. It was observed that the microstructure has a significant impact on the catalytic properties. Additionally, the possibility of $SmSrNiO_{4-\delta}$ thin films as Nanoelectrocatalyst and the impact of doping on electrode performance as a hybrid capacitor was also investigated. Previous research revealed that the Ni oxidation state varies from Ni^{2+} to Ni^{3+}, which was confirmed by XPS. This variation has a significant impact on the electrode's electrochemical behaviour. Therefore,

using the spin coating approach and altering the number of depositions from 1 to 6, we synthesized and characterized NiO thin films in order to better understand the functionality of

Ni. The substrate used for the deposition is silica. And report the structure, surface morphology and electrochemical properties in three different electrolyte media. NiO thin films exhibit impressive electrochemical behaviour and good crystallinity when specific circumstances are carefully optimized.

6.2 Synthesis and characterization of electrocatalyst

Thin film technology, which was used in this work, is a highly fascinating approach for electrocatalysis. In the past, a variety of approaches have been used to produce NiO thin films[271]–[275]. Due to a variety of benefits over conventional deposition processes, the sol-gel approach stands out among these techniques as a promising processing path. The benefits of sol gel approach are already discussed in chapter 2. Thus, in this study, sol-gel technology is used to create NiO thin films on a silica substrate. The precursor, solvent, and catalyst are Nickel acetate tetrahydrate, 2-methoxyethanol and Hydrochloric acid (HCl) of 0.1 mol of concentration respectively. For sol gel formation, 3.729 gram of Nickel acetate tetrahydrate was dissolved in 100 ml of 2-methoxyethanol and after that HCl was added drop by drop to this solution. This solution was continuously stirred for two hours at a constant temperature of 60 °C, result in a homogenous transparent solution of green color. The solution was left for 24h for at RT to obtain the sol-gel. For thin film deposition, Silica substrate was preheated for 5 minutes at temperature of 150 °C. it was also cleaned ultrasonically with ethanol, deionized water, and acetone, respectively, for 15 min each. The obtained cloudy green solution was filtered and spin coated (90µl) on Silica substrate at RT with spin coater by maintaining the spin rates 3500 rpm and spin time 30 seconds. Thin films were deposited on silica substate of different thickness by varying the number of deposited layers of nickel oxide. For multilayer depositions, thin films were dried for 5 min in air at 500 °C after each coating and the process

was repeat N times for N multilayers. Finally, all deposited thin films were annealed at the temperature of 500 °C and cooled down up to RT to obtain crystallized NiO. All the thin films are abbreviated as N_n (n varies from 1 to 6 indicates the deposited number of NiO layers). Therefore, these thin films will be mentioned as N_1, N_2, N_3, N_4, N_5, and N_6 respectively. AFM technique was used to roughly calculate the thickness of the two extreme samples namely N_2 and N_6. Surface morphologies are investigated by SEM and AFM. The crystalline growth has been confirmed at atomic level by AFM images. The phase formation is confirmed through an x-ray diffraction (XRD) technique using EQUINOX Laue X-ray diffractometer. The XRD pattern is well matched with the standards (JCPDS, #89-5881) confirm the formation of cubic structure with space group ($Fm\bar{3}m$, #225). Deposition of thin film was checked by optical microscope, which was further confirm by AFM by using the NTEGRA Prima instrument. The catalytic study of the sample was performed through cyclic voltammetry using Keithley 2450 source meter using three-electrode system. For three electrode system, Pt wire was used as counter electrode, Ag/AgCl was used as reference electrode. For working electrode, thin film was attached with copper wire making it insulating from outside. The concentration of electrolyte solution was 1 M for all three medias i.e., sodium sulfate (Na_2SO_4), KOH, and H_2SO_4.

6.3 Results and Discussion

6.3.1 Structural Studies

The XRD diagram of all the NiO thin films (abbreviated as, N_n (n = 1,2,3,4,5,6, indicates the number of NiO layers) that were deposited and annealed on the silica substrate at 500 °C is presented in figure 6.1. It confirms the formation of cubic phase with $Fm\bar{3}m$ symmetry and displays polycrystalline phase with the three strongest peaks, indexed as (220), (200), and

(111), matching with the standard JCPDS file (#89-5881). From Fig.6.1 we can see the amorphous nature of a silica substrate when seen at a lower angle i.e., 10 º < 2θ < 30 º followed by the crystalline phase of NiO. For further analysis we have chosen two nearly extreme cases i.e., N_2 and N_6. The XRD patterns are not horizontal for all the samples which indicates the presence of partial amorphicity (i.e., the background).

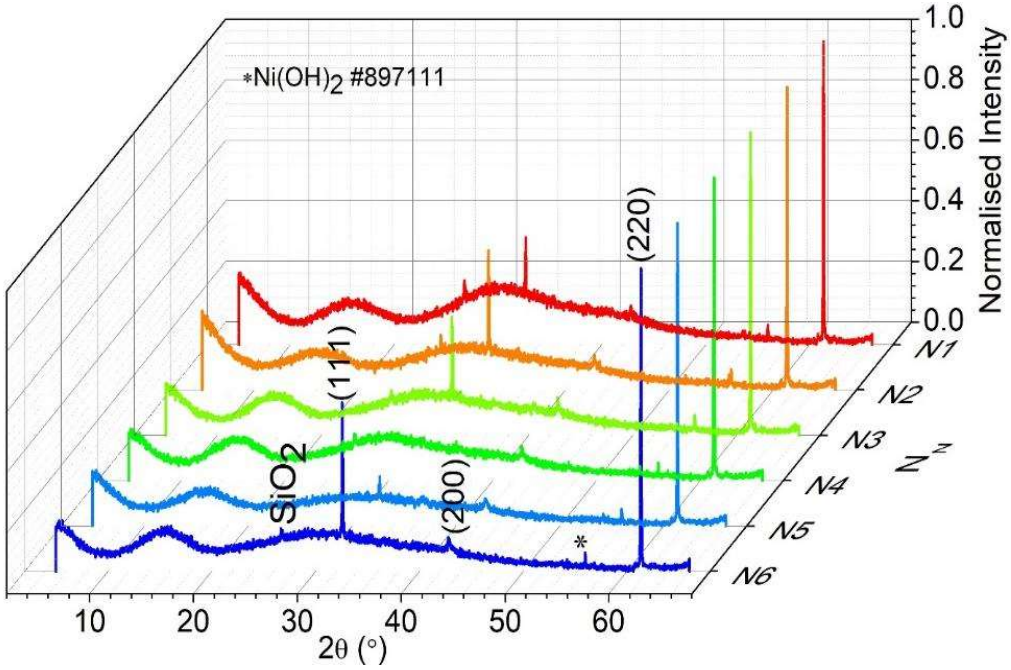

Figure 6.1: X-ray diffraction pattern of NiO thin films.

6.3.2 AFM and SEM studies

The surface morphology and roughness of films was investigated by Scanning electron microscopy (SEM) and atomic force microscope (AFM). SEM images for N_2 and N_6 samples are shown in (figure 6.2(a, b)). Two-dimensional AFM images are shown in (figure 6.2(c, d)) of films namely N_2 and N_6 which shows inhomogeneous surface made up of grains and voids. Figure 6.2(e, f) shows the 3D view of AFM images. The surface roughness for N_2 sample is ~ 0.01 nm and for N_6 is around ~ 0.6 nm, suggesting the surface of N_6 is rougher than N_2. AFM

images are used to estimate the approximate thickness of the samples, which are around ~50 nm for sample N_2 and ~90 nm for sample N_6. As we increase the number of deposited layers there is a sharp change in the height of peak can be seen from the 3D view of AFM images. SEM images revealed that the well-crystalline thin films formed under the current synthesis condition. This fact also agrees well with the XRD results. From SEM images it can be seen that films consists some overgrown clusters on the surface of film in sample N_2, while with increase in number of deposited layers the homogeneity and densification take place. Atomic concentration is also determine using SEM images and shown in (figure 6.2 (g)).

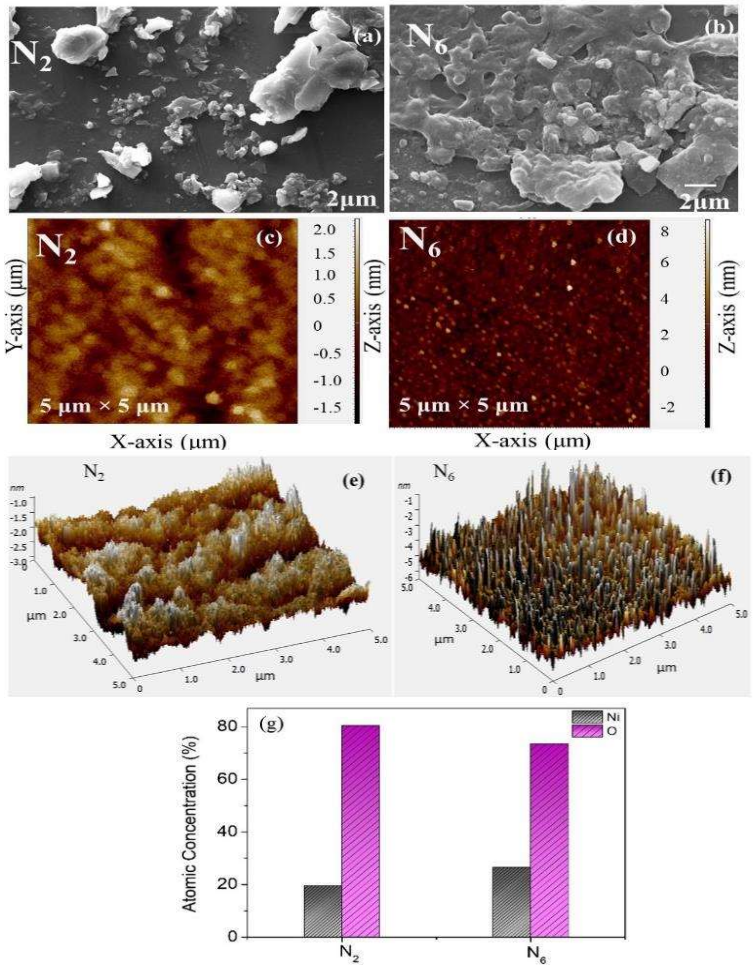

Figure 6.2: (a, b) SEM micrograph of sample N_2 and N_6 (c, d) Topographical AFM images of sample N_2 and N_6 (e, f) 3D images of AFM of both films (g) EDAX analysis of N_2 and N_6 thin films.

6.3.3 FTIR analysis

Figure 6.3 shows the FTIR transmittance spectra of NiO thin films of samples N_2 and N_6 with base line correction, which showed several significant absorption peaks over the spectral range of 550 to 4000 cm^{-1}. The Ni-O stretching vibration mode is attributed to the broad absorption band appeared in the region of (600-700) cm^{-1}, notably at 500 cm^{-1}; the broadness of the absorption band reflects the nanocrystalline structure of the sample. In both samples, the presence of the hydroxyl group is only visible above 2000 cm^{-1}[263][276].

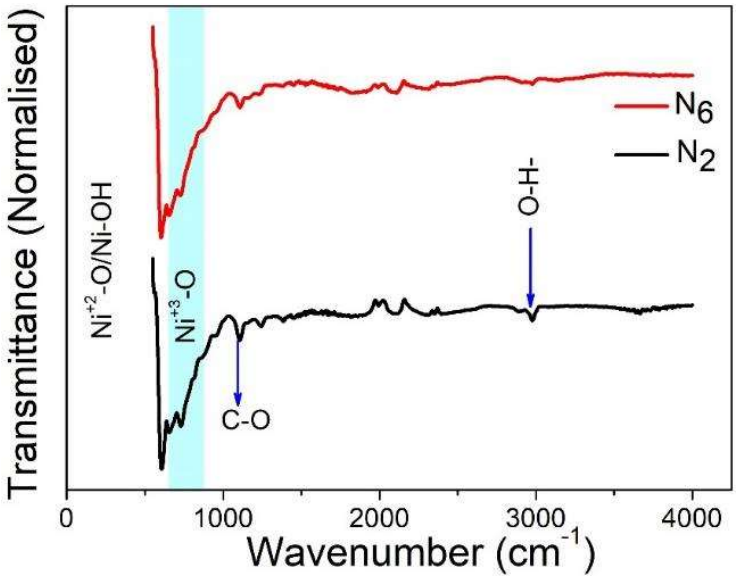

Figure 6.3: FTIR spectra of N_2 and N_6 thin films.

6.3.4 Electrocatalytic Studies

6.3.4.1. CV Curve analysis

Nickel is an important electrode material which is widely used in batteries, fuel cells, and alkaline water electrolysis in electrochemical Technology. The electrocatalytic activity of NiO was measured using a standard three-electrode system and in three different solutions Na_2SO_4 (neutral), KOH (alkaline), H_2SO_4 (acidic). The pH value of these electrolyte system was 7, 14, 1 respectively. All the electrolyte solutions have a concentration of 0.5M. NiO thin

films namely, N_2 and N_6 was used as working electrode, Ag/AgCl as reference electrode and pt wire as counter electrode. The working potential was observed with respect to Ag/AgCl and converted to reversible hydrogen electrode (RHE).

The Oxygen Evolution Reaction (OER) depends on pH of the solution. For all three mediums it occurs in different ways such as,

$$2H_2O \rightarrow O_2 + 4H^+ + 4e^- \qquad (6.1)$$

$$4\,OH^- \rightarrow O_2 + 2H_2O + 4e^- \qquad (6.2)$$

Equation 6.1 is for neutral and acidic mediums while equation 6.2 is for basic medium. Figure 6.4 shows that the different working potential window for OER and ORR obtained at different pH values. The CV response of Sample N_2 and N_6 recorded at the scan rate of 15 mV/sec in 0.5M (a) H_2SO_4, (b) Na_2SO_4, (c) KOH, respectively. It is observed that duck shape is featured in all three mediums for both samples. These duck shaped curves are a sign of catalytic regeneration of reactant near electrode. However, when assessing the value of current, it is observed to be highest in case of acidic medium rather than neutral and alkaline medium.

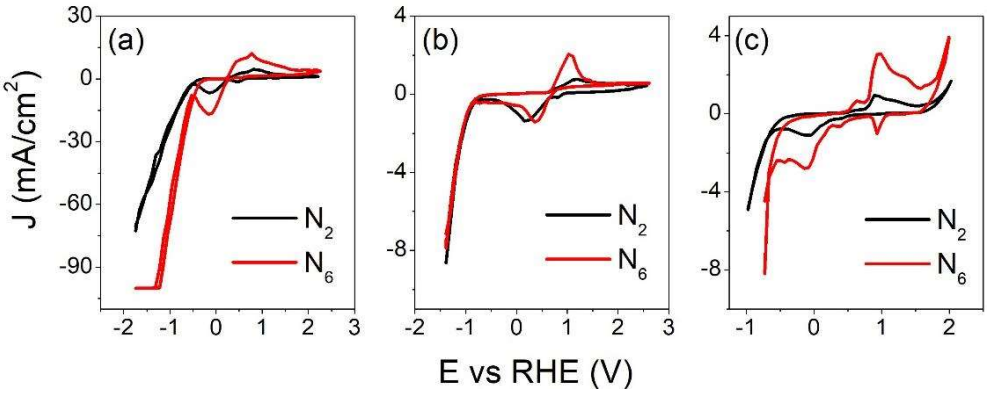

Figure 6.4: CV response of Samples N_2 and N_6 recorded at the scan rate of 15 mV/sec in 0.5M (a) H_2SO_4 (b) Na_2SO_4 (c) KOH media, respectively.

Additionally, when compared to N_2 samples, the area under the curve for N_6 is found to be higher. In addition to "duck" shaped feature, there is presence of kink in the voltammogram curves of the thin film in alkaline medium. This kink symbolizes the presence of multiple oxidation states that may be interconverted via electron transfer.

To observe the variation of area under the curve, the voltammograms at the lowest and highest scan rate is plotted for N_2 and N_6 samples as shown in figure 6.5. It is observed that shape of voltammogram is almost similar with the increase in area as the scan rates increases, for both the samples in all three media. The cyclic voltammograms with the variations of scan rate are depicted in figure 6.6. It is observed that with the variation of scan rate, the peak position is found to move towards higher current and higher voltages. The increase in current with the scan rate is a common observation is basically due to the reduction in the size of diffusion layer as the scan rate increases. Peak-to-peak separation seems to shift with the scan rate in all the samples, confirming one electron transfer between the analyte and the electrode.

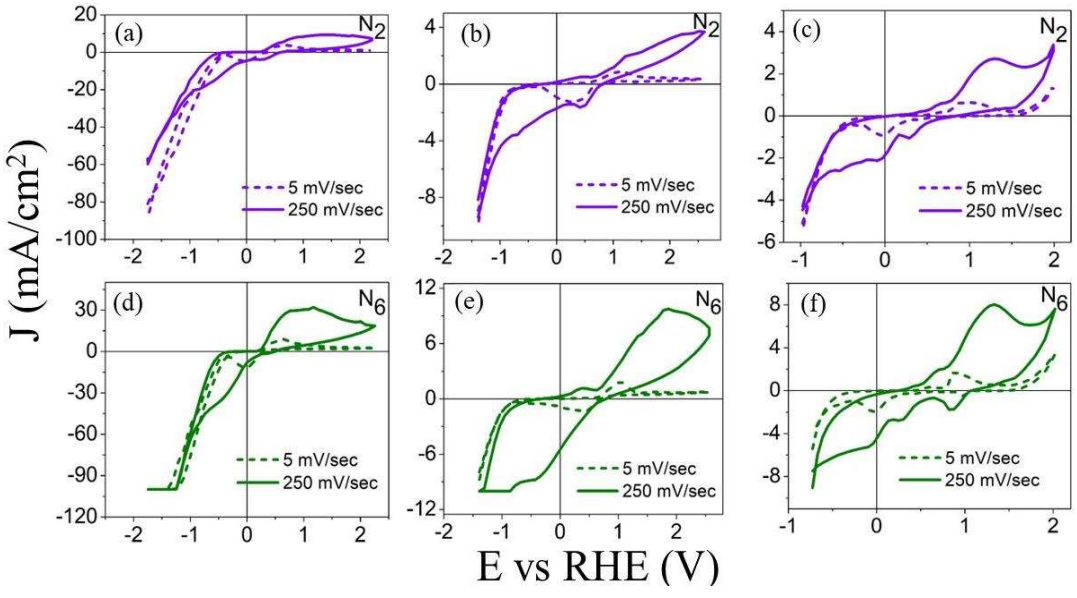

Figure 6.5: Variation of area of voltammograms with the scan rate for N_2 and N_6 in 0.5M (a, d) H_2SO_4 (b, e) Na_2SO_4 (c, f) KOH media, respectively.

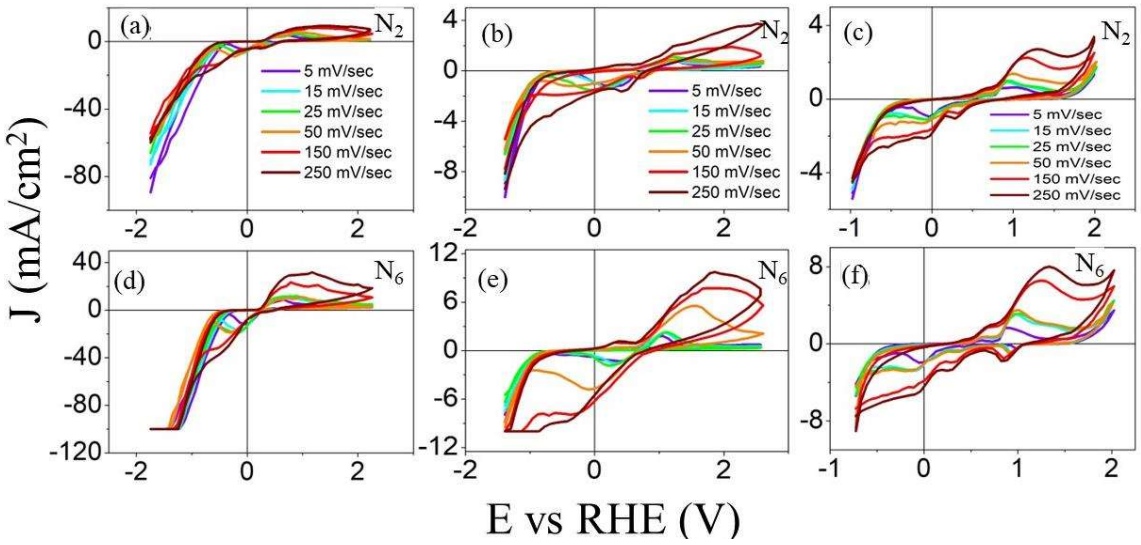

Figure 6.6: Cyclic Voltammetric curves for N_2 and N_6 at different scan rates in 0.5M (a, d) H_2SO_4 (b, e) Na_2SO_4 (c, f) KOH media, respectively.

In order to check the reversibility of the electrode reactions, the difference between the cathodic and anodic peak (ΔE_p) is calculated for all the samples at a scan rate of 15 mV/s (figure 6.7).

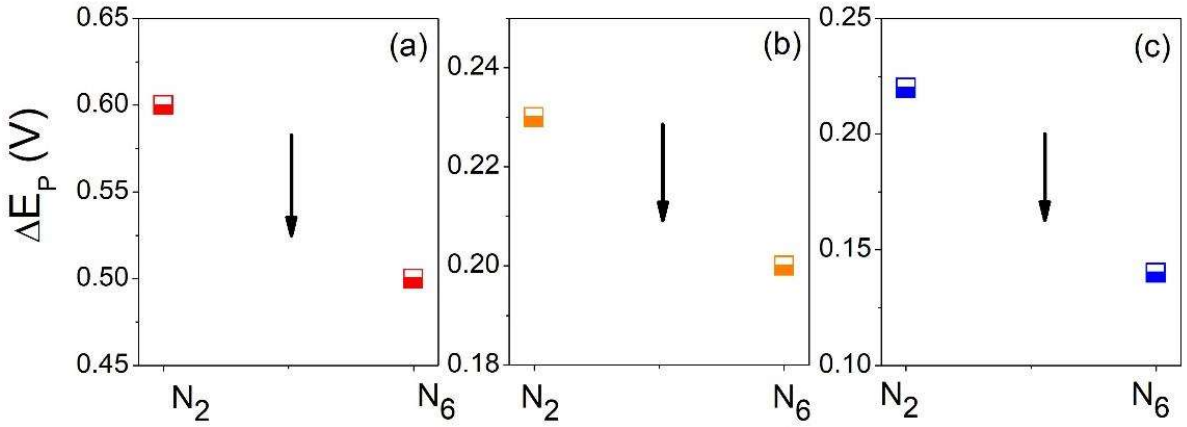

Figure 6.7: Peak to peak separation ΔE_P observed at the scan rate 15 mV/sec for N_2 and N_6 in 0.5M (a) H_2SO_4 (b) Na_2SO_4 (c) KOH media, respectively.

From figure (6.7) it is clear that for sample N_6 the peak-to-peak separation is less than sample N_2 in all three media with a minimum of 0.14V for sample in KOH medium, representing its better reversibility towards electrochemical reactions.

As shown in figure (6.8), the peak current density has also been determined to understand the electrochemical activity of both the samples N_2 and N_6. The peak current density for sample N_6 is higher than sample N_2 in all three media, with acidic H_2SO_4 medium having the highest value (11.58 mA/cm^2), indicating sample N_6 higher catalytic activity than N_2[277]. During the catalysis process $Ni(OH)_2$ phase involves in the OER mechanism (confirmed through XRD) in order to promote the charge transfer during the reaction mechanism.

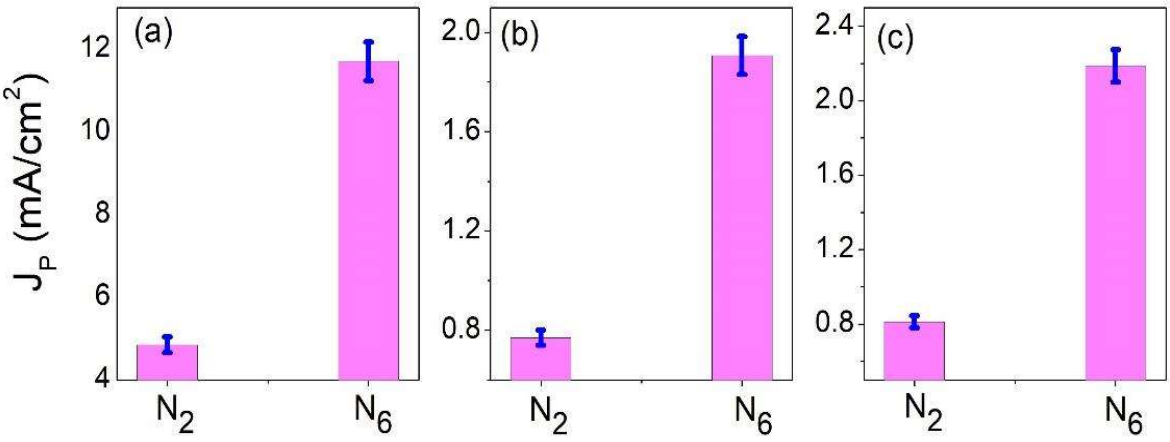

Figure 6.8: Peak Current density observed at the scan rate 15 mV/sec for N_2 and N_6 in 0.5M (a) H_2SO_4 (b) Na_2SO_4 (c) KOH media, respectively.

6.3.4.2 RS equation

In cyclic voltammetry, electrochemically reversible process with freely involved redox carriers are employed using Randles-Selvick (RS) equation, already mentioned in previous chapter. For electron absorbed species, this equation shows a liner behaviour between the

cathodic current and root value of scan rate. RS equation in this case is modified as $i_p = \frac{n^2F^2}{4RT} vA\Gamma^*$. Here n represent the total number of electrons involved in the redox reaction, v denotes the scan rate, T is Temperature (Kelvins) ,F is faraday constant, , R is the universal gas constant, A represent the electrode surface area, and Γ^* is the surface covered under adsorbed surfaces[278]. To describe peak behavior, peak current is plotted versus $v^{1/2}$ (Figure 6.9). The plot of RS equation is linear for all the sample, indicating the quasi-electrochemical reversibility with the freely diffusing redox species.

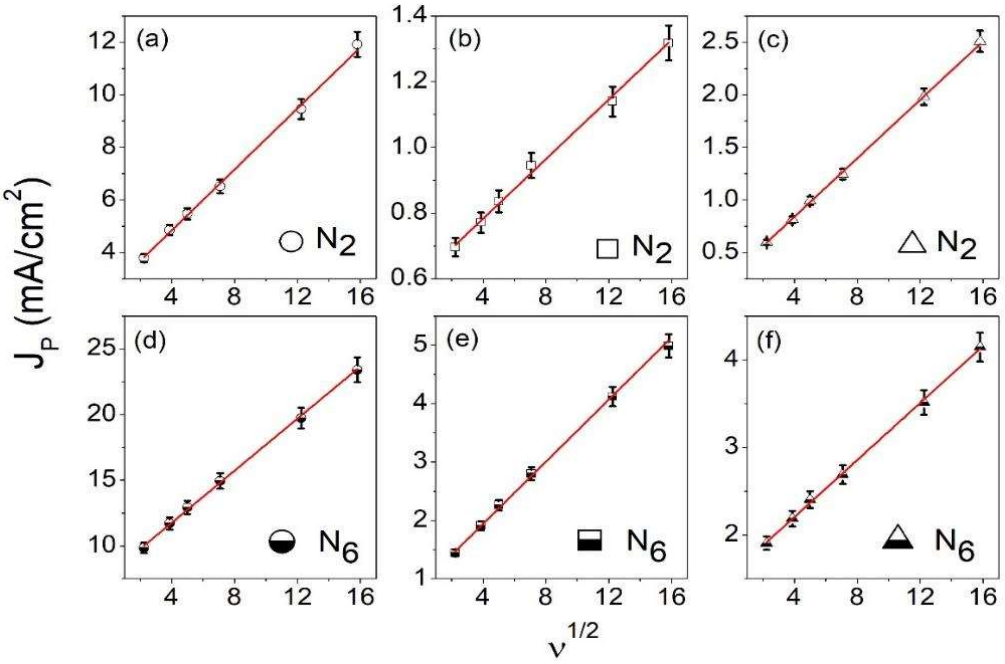

Figure 6.9: Variation of j_p vs $\upsilon^{1/2}$ as per RS equation for N_2 and N_6 sample in 0.5M (a) H_2SO_4 (b) Na_2SO_4 (c) KOH media, respectively.

6.3.4.3 Specific Capacitance:

The value of Specific capacitance is estimated for both the samples by using the formula

$$C_p = \frac{\int I(v)dv}{mv\nabla V} \qquad (6.3)$$

Here, $\int I(v)dv$ represent the area under the curve in CV graph, m is the mass of the active electrode (in gm), ∇V is the potential window (-1.5 V to +1.5 V), ν indicates the scan rate. The variation of specific capacitance with scan rate for both the samples N_2 and N_6 is shown in figure 6.10. The value of specific capacitance decreases with scan rate is a well-known process, the de- Levie effect of electrode, as mentioned in the previous chapter as well. The highest value is observed in acidic medium, followed by the alkaline and neutral medium. On a comparative note, N_6 shows the better value of specific capacitance in all three media as compared to the N_2 sample. The high value of specific capacitance indicates that N_6 has maximum reversible redox process for charge storage as well as diffusion and ion penetration for faster electrode kinetics as compared to the N_2 sample.

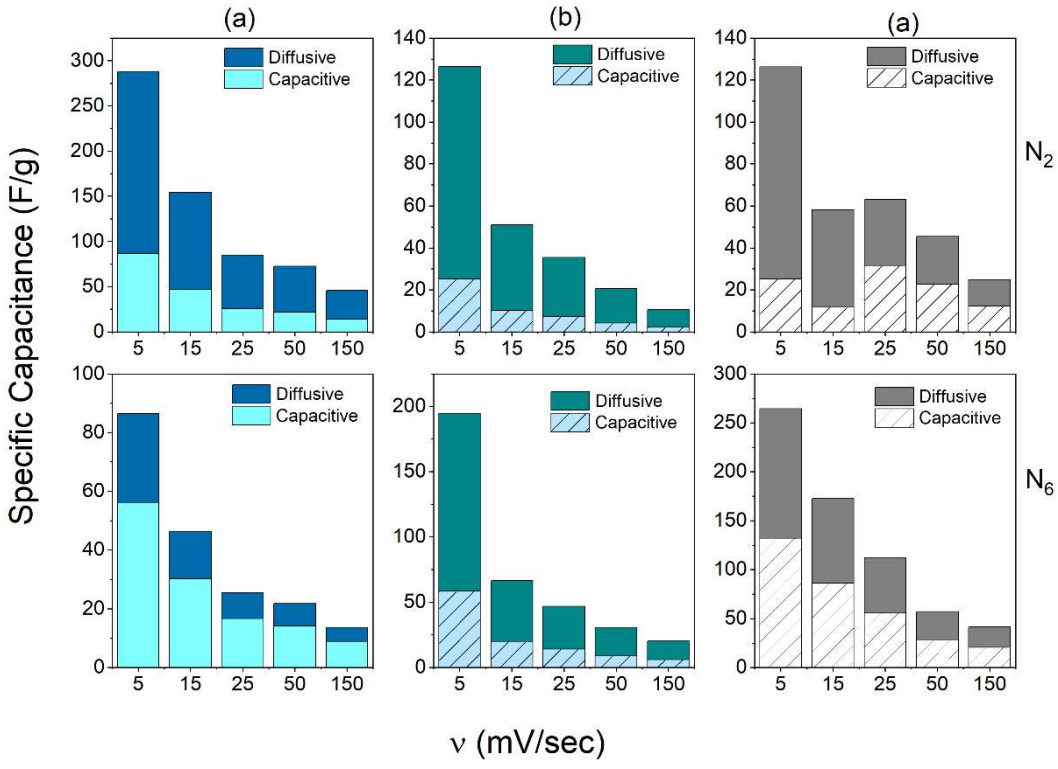

Figure 6.10: Variation of Specific capacitance with scan rate for N_2 and N_6 samples in 0.5M (a) H_2SO_4 (b) Na_2SO_4 (c) KOH media, respectively.

6.3.4.4 General Power Law:

The general power law relationship gives the information regarding the total charge storage process in electrode system. This relationship is given as per the equation:

$$i = av^b \qquad (6.4)$$

Here, i represent the total current, ν is the scan rate and a and b are the constants. The value of b gives important kinetic information about the electrochemical reactions. The process is a diffusion-controlled faradic process if the value of b is equal to 0.5. If b is equal to 1, this indicates that fast near-surface processes are the major contributor. The electrode process is under mixed control diffusion if the value of b is between 0.5 and 1, and these activities can be EDLC charging or discharging or rapid surface redox reaction[240]. The value of b is calculated for both samples in all three media and shown in figure 6.11. it is found that the value of b for N_2 in all medium is below 0.50, for which there is no define parameter.

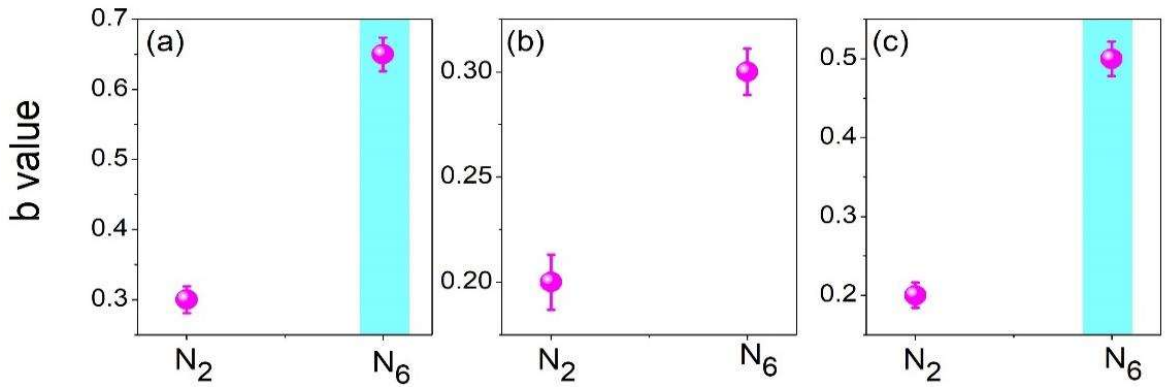

Figure 6.11: b-value plotted for N_2 and N_6 in 0.5M (a) H_2SO_4 (b) Na_2SO_4 (c) KOH media, respectively.

However, for N_6, the value of b is lie between 0.50 to 1.0 indicating the presence of mixed control of faradic and non-faradic process in acidic medium. In alkaline medium, the value of

b is almost 0.50 indicative the diffusion-controlled ion or electron transfer processes and current is mostly comes from pseudo-capacitive process.

6.3.4.5 Electrochemical double layer capacitance

This is also another important parameter of oxygen electrodes which signifies the electrochemically active surface area (ECSA) of the catalyst for catalytic activities. For electrodes N_2 and N_6 the value of C_{dl} was calculated in non-faradic region[245] and shown in figure (6.12) in all three media. It is observed that C_{dl} value for samples N_6 is higher in all three media as compare to the sample N_2 with highest value in alkaline medium i.e., 46.1 mF/cm^2, showing high active surface area. The value of Cdl is supporting the behaviour observed in general power low. This is indicating that N_6 sample is more feasible for catalytic activity in alkaline medium.

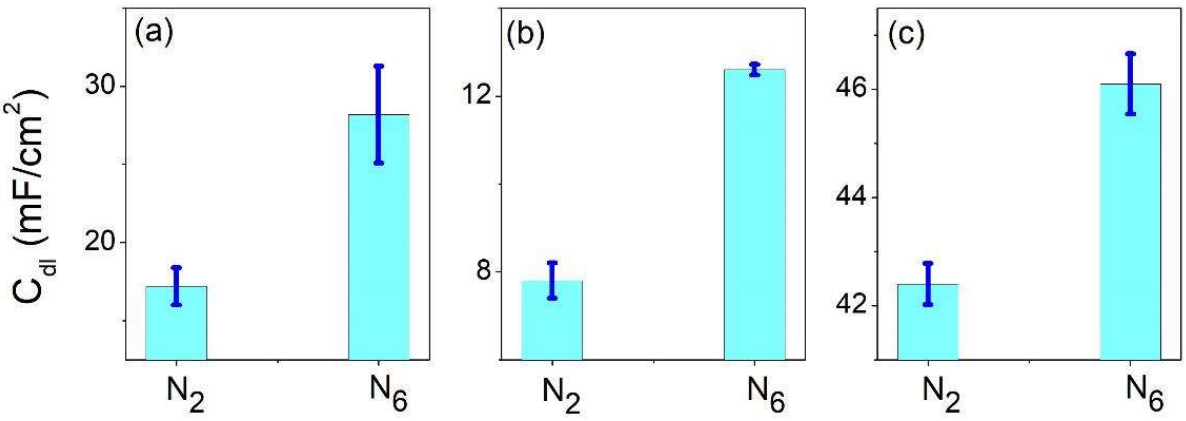

Figure 6.12: C_{dl} value for N_2 and N_6 electrodes in 0.5M (a) H_2SO_4 (b) Na_2SO_4 (c) KOH media, respectively.

6.3.4.6 Tafel slope

Tafel plot is basically used to calculate the corrosion rate (CR) and tafel slope. The equation which is used to calculate is CR (mm per year) = $3.27 \times I_{corr} \left(\frac{mA}{cm^2}\right) \times \left(\frac{ew}{d}\right)$, where ew is the equivalent weight, I_{corr} is the corrosion current, and d is the density of the material.

Tafel slope is charge transfer rate determining step. The tafel slope has calculated for both N_2 and N_6 samples in all three mediums and shown in figure 6.13. The different corrosion rates of N_2 and N_6 corresponds to the different passivation mechanism and thickness of protective layer which develops over the electrode. For N_2 and N_6, the tafel slope in an acidic medium is ~ 90 mV/decade, whereas in a basic or neutral mediums, it is roughly ~140 mV/decade. Tafel slope is believed to be affected by the pH of the solution and analyte concentration. So, in alkaline medium value of tafel slope confirms that the ORR takes place through $4e^-$ pathways, while it occurs through $2e^-$ pathways in basic and neutral mediums[229].

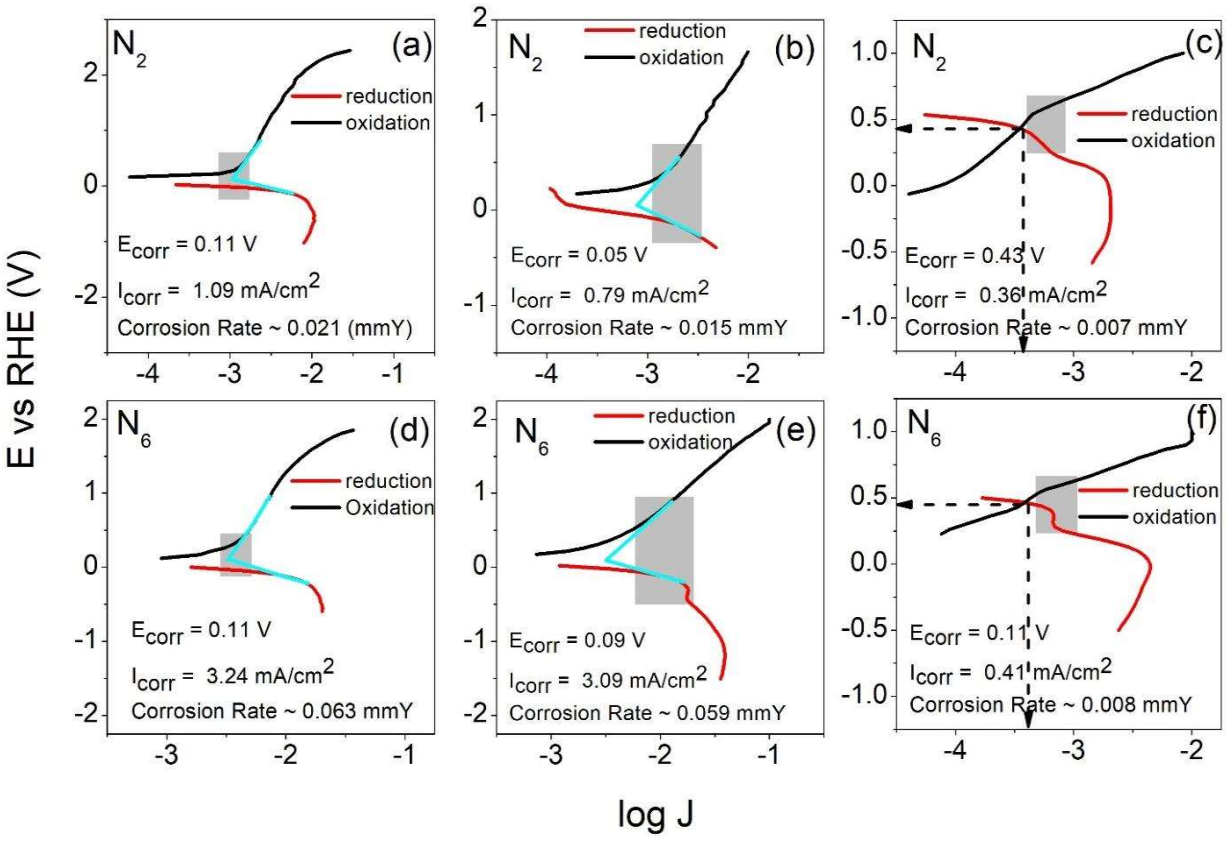

Figure 6.13: Tafel plots for N_2 and N_6 electrodes in 0.5M (a, d) H_2SO_4 (b, e) Na_2SO_4 (c, f) KOH media, respectively. Grey part presents the range where tafel slope is calculated.

6.3.4.7 Chronoamperometry study

The chronoamperometric response of both the sample is evaluated to check the stability and evaluate transient current decay time (Fig. 6.14). For this we have chosen the environment friendly medium Na_2SO_4. The transient current decay time is estimated by fitting the current vs time graph (Fig.6.14) with the exponential decay equation. The decay time is almost same for both the sample. The decay time is observed ~54 sec for N_2 sample and ~57 sec for N_6 sample. Both the sample shown a stability for over a long time of period of 4000 seconds. This indicates the suitability of both the samples for electrocatalysis process.

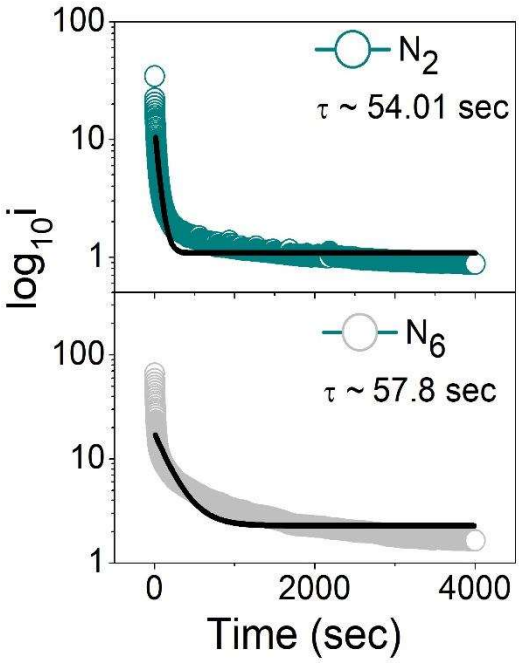

Figure 6.14: Chronoamperometric response for N_2 and N_6 in 0.5M Na_2SO_4 medium

6.4 Conclusion

Thin films of NiO are prepared by using the sol gel method on silica substrate. By varying the number of deposited layers from N = 1 to N = 6 we have prepared six samples namely N_1, N_2, N_3, N_4, N_5, and N_6 of different thickness. The XRD patterns confirm the cubic phase with

$Fm\bar{3}m$ symmetry and displays polycrystalline phase. AFM and SEM confirms the well grown thin films on silica substrate. Electrocatalytic study was performed by using the cyclic voltammetry and further analyses was done on two extreme sample namely N_2 and N_6. The existing $Ni(OH)_2$ phase act as catalytic mediator in OER reaction which enhances the electrocatalytic activity in alkaline medium. Tafel slope confirms that in acidic medium ORR takes place through $4e^-$ while in basic and neutral medium it happens through $2e^-$ pathways. The value of specific capacitance is promising for the sample N_6 as compared to the N_2. It was found that thin film with highest number of deposition (i.e., N_6) shows promising behavior as electrocatalyst in alkaline and acidic mediums.